

Review

Bonding Analysis of Compounds with Unusual Coordination of Carbon: Proposed Symmetric Systems with Six-Coordinate Carbon

Carl Trindle ^{1,*} , Zikri Altun ²  and Erdi Ata Bleda ² ¹ Chemistry Department, University of Virginia, Charlottesville, VA 22904, USA² Physics Department, Marmara University, Istanbul 34724, Turkey; zikalt@marmara.edu.tr (Z.A.); ata.bleda@marmara.edu.tr (E.A.B.)

* Correspondence: cot@virginia.edu; Tel.: +1-434-770-9197

Academic Editor: Steve Scheiner

Received: 21 July 2020; Accepted: 26 August 2020; Published: 28 August 2020



Abstract: The possibility of carbon tetravalence in geometries other than tetrahedral and of carbon hypervalence has been taken seriously since the 1970s. Computational modeling and subsequent experimental validation have established the existence of molecules with carbon atoms with planar tetravalence and as many as six objects in carbon's coordination sphere. In this work, we develop insight into the nature of bonding to carbon in these unusual environs as provided by Bader's Atoms in Molecules (AIM) analysis of the electron density, along with the electron localization function (ELF) and the non-covalent index (NCI). We review several well-established systems (spiropentadiene dication, hexamethyl benzene dication, dimethanospiro[2.2]octaplane dication, and 1,8-dimethoxy-9-dimethoxyanthracene cation) and propose new D_{2d} -symmetric variants of a hexacoordinated species.

Keywords: AIM modeling; electron localization function; non-covalent interaction; carbon hypercoordination

1. Introduction

One of the basic insights of organic chemistry is that saturated carbon atoms arrange four partners in tetrahedral coordination. [1–4] Lewis electron pairing and the Valence Shell Electron Repulsion model [5,6] reinforce the insight, allow easy applications, and shape our intuition. Minor departures from the ideal form can be interpreted as a consequence of the lower symmetry of the arrangement of the four objects in the coordination sphere. But major departures from tetrahedral tetracoordination—that is to say, either serious change as from (a) tetrahedral to planar four-coordination or (b) hyper-coordination with five or more neighbors—are rare, and require special explanation.

The instability of planarized tetracoordinate carbon as in planar methane (called tpC₁) is attributed to its nonbonding pi lone pair [7,8]; in the tetrahedral form all four valence pairs participate in bonds. Planarity can be enforced by two kinds of influence: (1) Removal of the pair of electrons that destabilize the planar form, first exemplified in the discussion of planar methane [7]; (2) ring strain; and/or (3) suitable substitution and associated electronic effects. For example, the closed-shell ground state dication of CH₄ is planar (qualitatively, a C_{2v} complex of H₂ with CH₂ dication) [9]; the double ionization removes charge from the p-pi AO of the Carbon. We discuss structures for other dications with unusual coordination of a central carbon atom, notably 1–4 (Figure 1). The dication of spiropentadiene (1) is D_{2h} in symmetry, as modeled computationally by Lammertsma and Schleyer [10]. The pentagonal-pyramidal structure of hexamethylbenzene 2 is achieved only in the dication, established experimentally by Hogeveen et al. [11–13].

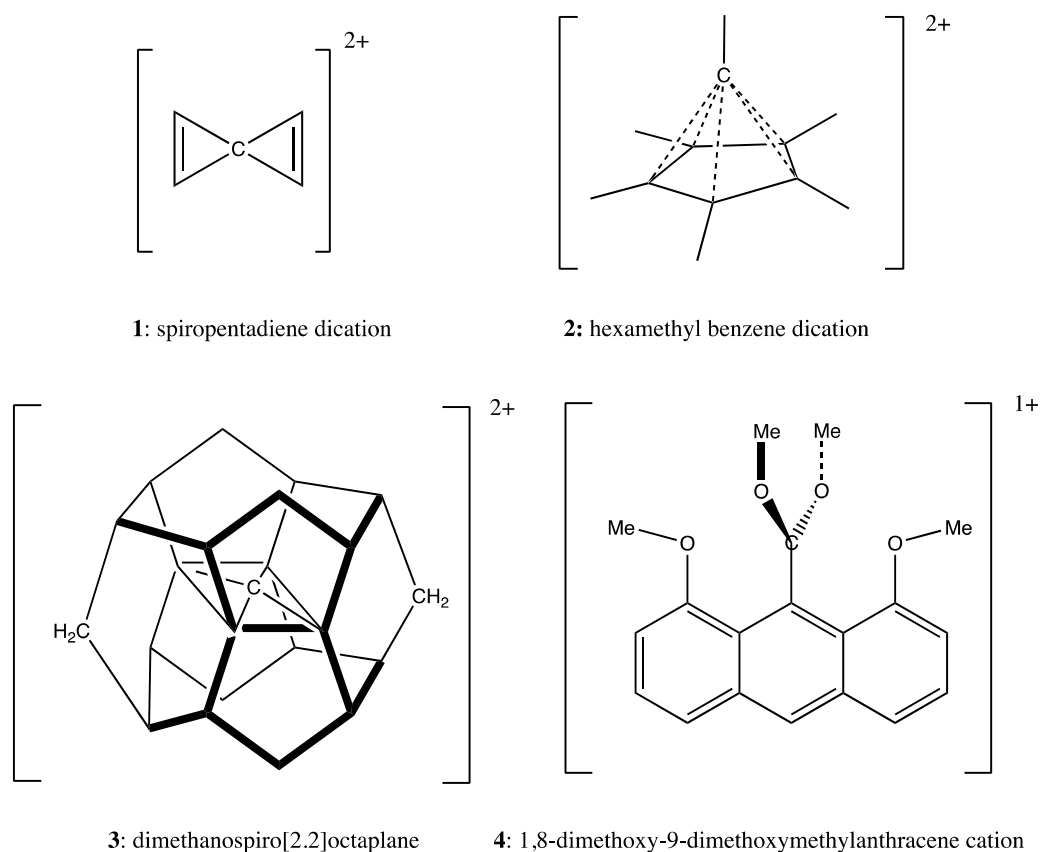


Figure 1. Notable structures with unusual coordination of carbon.

Radom's alkaplane systems [14] rely entirely on strain to force the central CC_4 fragment toward planar tetracoordination of Carbon. The tpC with its immediate C neighbors in D_{2h} dimethanospiro[2.2]octaplane 3 is shown in Figure 1. However, the stability of the neutral D_{2h} -symmetric form is questionable. Radom and Rasmussen [14] report that a MP2/6-31G(d) calculation (by Mark S. Gordon, unpublished) produces all-real vibrational frequencies, suggesting the D_{2h} structure occupies a relative minimum on the potential surface. B3LYP/6-31G(d) calculation and our ω B97XD/cc-pVTZ calculation both produce a substantial imaginary frequency (ca. 300i) suggesting the symmetric form is a transition state between two twisted forms of the CC_4 fragment in the dimethanospiro[2.2]octaplane. Figure 2 displays the isosurface of the HOMO for neutral 3, which is dominated by the troublesome C lone pair. This form of the HOMO is in general agreement with results of calculations at lower levels of theory [14,15].

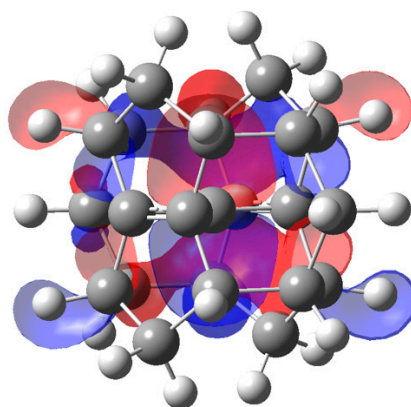


Figure 2. HOMO for neutral dimethanospiro[2.2]octaplane.

The planarity can be established by ionization; the monocation radical has a planar tpC [15]. We have confirmed that complete removal of two electrons from the HOMO more firmly establishes stability of the D_{2h} symmetry of Radom's dimethanospiro[2.2]octaplane dication.

Substitution of two Carbon atoms by Boron atoms, forming systems isoelectronic with the hydrocarbon dications, accomplishes planarization. This formation of neutral analogs to hydrocarbon cations is called the charge compensation principle by its inventors [13] and is applied to this issue by Wang and Schleyer [16]. A tactic recommended by Hoffmann [7,8] is to surround the central carbon by species which are strong sigma donors and pi acceptors, which then may effect redistribute the troublesome planar-Carbon lone pair toward its surroundings. A series of molecules incorporating Copper and Nickel substituents on the tpC investigated by Schleyer and Boldyrev [17] reverse this motif, calling for strong pi-donor and sigma-acceptors on a periphery. A central example is CAI_4 anion [16]. Structures with many other metals have been evaluated computationally [18–21].

The same stratagem has prompted computational studies of planar penta- and hexa-coordinated Carbon. For example, Exner and Schleyer [22] used B3LYP and CCSD(T)/6-311+G(d,p) to describe a planar CB_6^{2-} system as well as isoelectronic and neutral C_3B_4 and other variants.

In this report we confine our attention to metal-free systems and examine hypercoordinated Carbon atoms with O and S members in the coordination sphere. The coordination sets in our systems are often nonplanar. Our purpose is to characterize the interactions of the hypercoordinated carbon with its neighbors. To assist intuition we employ diagnostics and visualization aids from Bader's Atoms-in-Molecules theory [23], and related quantities such as the electron localization function [24] and the non-covalent index [25].

2. Computational Methods and Software

2.1. Software

We use Gaussian 09 [26] and 16 [27] for electronic structure calculations including geometry optimization and vibrational analysis. The density functional model is ω B97XD [28] and the basis is cc-pVTZ [29] except as otherwise noted. With one exception (5) in which the experimental (X-ray) structure is used, all reported structures are local minima according to ω B97XD/cc-pVTZ, with no imaginary vibrational frequencies. Bader AIM analysis is conducted by AIMALL [30] and Multiwfn software [31]. Construction of the electron localization function (ELF) and the non-covalent index (NCI) is accomplished with Multiwfn and NCIplot [32]. In the following sections we describe AIM, ELF, and NCI methods of characterizing the electron density. Those familiar with these analyses may wish to pass directly to Section 3, in which we describe applications.

2.2. AIM and Bader Terminology

The Atoms-in-Molecules (AIM) analysis characterizes bonding with reference to the electron density, an observable of a molecular system. The review by Kumar et al. is a useful introduction, with many examples [33]. At critical points where $\nabla\rho = 0$ we can evaluate the charge density ρ , its Laplacian $L = \nabla^2\rho$, and the eigenvalues $\{\lambda_k\}$ of the matrix $\{H_{ij}\} = \{\partial^2\rho/\partial x_i\partial x_j\}$ along with various energy densities. Diagonalization of \mathbf{H} yields three eigenvalues. There can be three negative eigenvalues, defining NCP nuclear critical points (attractors) coded (3, -3); two negative and one positive value defining BCP bond critical points, coded (3, -1), one negative and two positive values defining RCP ring critical points coded (3, +1), or three positive values defining CCP cage critical points coded (3, +3). The number of critical points of all kinds should obey the Poincare-Hopf rule, which in this case requires that $NCP - BCP + RCP - CCP = 1$. This is the case for all systems described here.

AIM divides Cartesian space into basins, each containing an attractor—most often a nucleus. The boundaries of the basins are defined by a zero-flux ($\nabla\rho = 0$) surface. Integration of electronic charge within a basin including a nucleus produces an AIM atomic charge.

For familiar covalent chemical bonds, the electron density ρ at a BCP would be on the order of tenths of density units, electrons per cubic bohr. For weak mainly electrostatic interactions such as H bonds, the density at the BCP would be much smaller (at best, hundredths of atomic units) and the Laplacian would be positive. In all the examples to follow, we find the usual array of nuclear attractors with very large densities and large negative Laplacian values; BCPs for covalent sigma bonds; nonpolar aromatic CC bonds in the anthryl rings; and polar bonds with smaller densities. In AIM analysis the kinetic and potential energy densities G and V at the bond critical points offer insight into the nature of bonding. A useful diagnostic of covalent bonding is the ratio $|2G(\mathbf{r}_{\text{bcp}})/V(\mathbf{r}_{\text{bcp}})|$; if this ratio is less than unity then the interaction is covalent [34].

While AIM provides a well-defined methodology for processing molecular electron density (obtained either by theoretical methods or by processing experimental data) its link to intuitive chemical constructs—especially bonds and atomic charges—has been the subject of considerable debate. We refer to only a very small sample, which will convey the flavor [35–38]. We judge that *reductio ad absurdum* does not undermine the practical value of QTAIM.

2.3. ELF

The electronic localization function (ELF) was defined by Becke and Edgecombe [24]. The probability density that a second like-spin electron is found near a “localized” electron is presumably small. This density arising from Fermions in the molecular system is written as:

$$D = \sum_i^\sigma |\nabla\psi_i|^2 - |\nabla\rho(r)|^2 / 4\rho(r) \quad (1)$$

The sum is over all the occupied molecular spinorbitals; $\rho_\sigma(r)$ is the electron density of electrons with σ spin which in the Kohn–Sham approximation is given by $\rho_\sigma(r) = \sum_i^\sigma |\psi_i|^2$. The smaller the quantity D , the more highly localized is the reference electron. A dimensionless index χ is defined as the ratio of the density D to the corresponding value for the uniform electron gas:

$$D_0 = \frac{3}{5}(6\pi^2)^{2/3} \rho^{5/3}. \quad (2)$$

ELF is confined to the range $[0, 1]$ by the transform $\text{ELF} = 1/(1 + \chi^2)$. The limit of maximum localization is $\chi = 1$.

2.4. NCI

A useful description of the non-covalent index, its graphical characterization, and its interpretation is given by Contreras-Garcia, et al. [39]. The reduced (dimensionless) density gradient s (also called RDG) is defined as

$$s(r) = \frac{|\nabla\rho(r)|}{2(3\pi^2)^{1/3} \rho(r)r^{4/3}} \quad (3)$$

Two NCI graphic realizations are useful. A two-dimensional plot of s vs. the density ρ (given the sign of the second eigenvalue of \mathbf{H}) will produce a broad sweep from one extreme at small density but large s to large density and small s . This is characteristic of an exponentially-decaying density. Superimposed on this sweep may be spikes in s extending to values near zero at modest values of density. In Figure 3, plots derived from $\omega\text{B97XD/cc-pVTZ}$ computations for water dimer and formic acid dimer are shown. The high-density (but low s) regions near nuclei are far to the right or left of the range of densities shown. The low-density region is located primarily in Cartesian space close to the density tails for which s is large. However, s can be small precisely where the density is disturbed by non-covalent interactions, such as van der Waals/dispersion and electrostatic forces. Figure 3 shows the plot for water dimer and formic acid dimer. For water dimer, we find one such case at signed density about -0.025 , and for formic acid dimer we find two, at $+0.01$ and -0.05 .

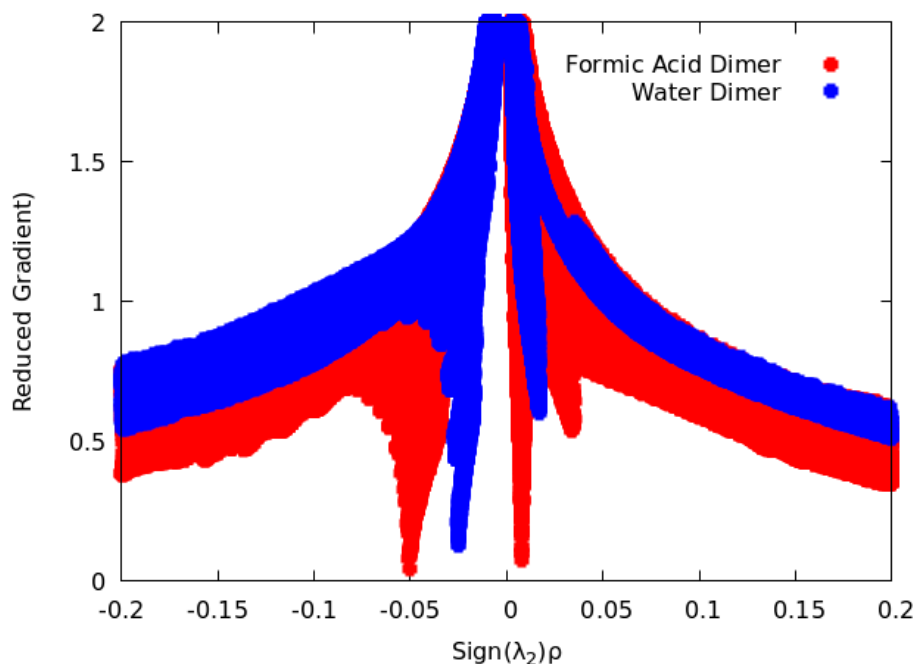


Figure 3. Two-dimensional representation of non-covalent interactions for water dimer and formic acid dimer.

Mapping those zones of small density and small s (RDG) into three-dimensional space (Figure 4), we isolate regions of significant NCI in isosurfaces of value 0.05. For water dimer there is a single zone of non-covalent interaction, which we must associate with H-bonding. One spike from Figure 3 can refer to more than one zone. In the formic acid dimer (Figure 4), we find two attractive H-bonding NCI regions and also a destabilizing zone corresponding to a ring critical point.

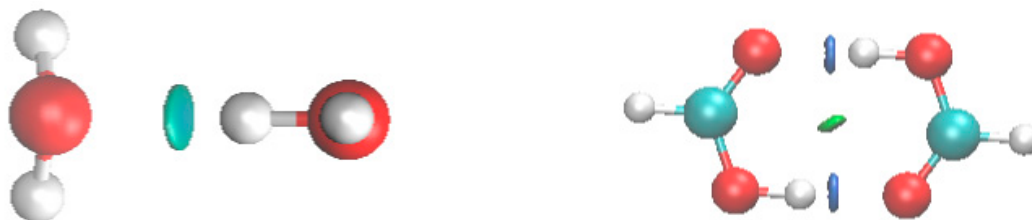


Figure 4. Zones for which both reduced density gradient (RDG) and density are small for water dimer (L) and formic acid dimer (R).

3. Density Analysis for Known Examples of Unusual Coordination of Carbon

3.1. Example 1: Spiropentadiene Dication

Our ω B97XD/cc-pVTZ calculations and earlier reports [10] verify that D_{2h} -symmetric spiropentadiene dication **1** occupies a relative minimum energy point. (The unsubstituted monocation and neutral counterparts however are nonplanar.) The neutral system can be constrained to coplanarity of the three-membered rings by enclosing the spiropentadiene core within aromatic seven-membered rings [40]. In this case the troublesome electron pair is exported from the p-pi AO of tpC into the aromatic region.

3.1.1. AIM Analysis

Firme et al. [41,42] presented an AIM analysis of the planar dication of spiropentadiene. Critical points and bond paths from our AIM2000 analysis of the density obtained with ω B97XD/cc-pVTZ are

shown in Figure 5. Values of density, the Laplacian, G and V at selected BCPs are shown in Table 1. Entries in red are from Firme, et al. [41] and agree pretty nearly with our ω B97XD/cc-pVTZ values. We see that the BCPs along the paths from a peripheral Carbon to the tetracoordinate planar Carbon have much smaller values of the Laplacian of the density compared with the values at BCPs along the two bond paths connecting peripheral C-Cs. We infer that the tpC-Cx bond is weaker than the Cx-Cx bond. It is remarkable that the tpC is has a net negative AIM basin charge (-0.193 absolute electrons or $|e|$); the positive charge in this dication is dispersed to the surrounding C and H atoms ($+0.169$ and $+0.379 |e|$ respectively.)

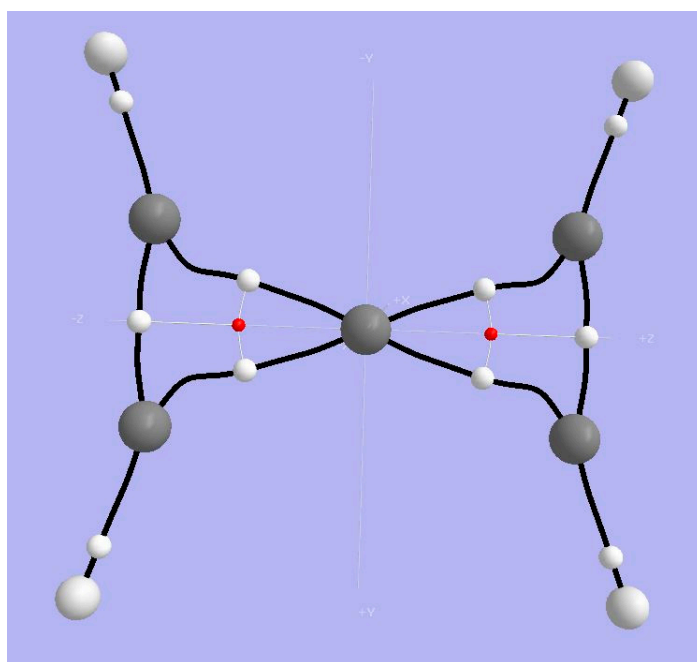


Figure 5. Topological (Bader) analysis of spiropentadiene dication 1. Large light-gray spheres = H atoms; large dark gray spheres = C atoms; small white spheres = BCPs; small red spheres = RCPs; black lines = bond paths.

Table 1. Selected AIM parameters for spiropentadiene dication. Cx is a peripheral Carbon, tetra-coordinate carbon as in planar methane (tpC) is the tetracoordinate planar Carbon. Red: From Firme et al. [41].

Critical Point	Density ρ	Laplacian	G	V	$ 2G/V $
tpC-Cx: (3, -1)	0.2323 0.230	-0.1184 -0.113	+0.1685	-0.3506	0.961
Cx-Cx (3, -1)	0.3708 0.369	-1.1167 -1.109	+0.1872	-0.6535	0.573
Cx-H (3, -1)	0.2716 0.275	-1.0302 -1.050	+0.0134	-0.2844	0.094
Basin Charges					
Charge ($ e $)	H = +0.3794	Cx = +0.1691		tpC = -0.1932	

3.1.2. ELF Analysis

The electron localization function shown in Figure 6 displays the four bonding regions C to H and the two single CC bonds, top and bottom. The pi character of the C=C bonds is visible at the bottom. The ELF zones for the CH bonds are extensive, compared with CC bonds. From the AIM basin charges, (Table 1) it appears that upon double ionization electron density from the HC=CH fragments has migrated so that tcC obtains a net negative charge.

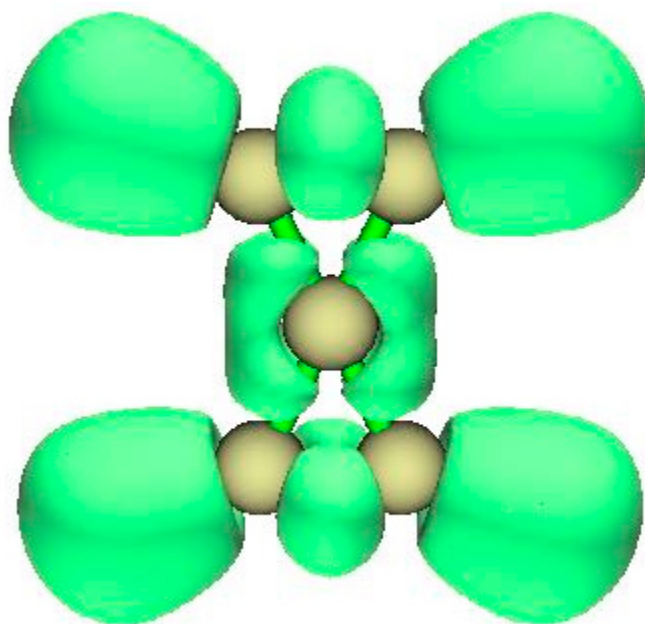


Figure 6. Electron localization function (ELF) for spiropentadiene (view perpendicular to D_{2h} plane).

3.1.3. NCI Analysis

The plot of the reduced density gradient $s(\rho)$ against the density as signed by the second eigenvalue of the Laplacian of the density shows no departures from monotone decline in $s(\rho)$ at left and right (See Figure S1, Supplementary Materials). That is, there are no zones of non-covalent interaction in this dication.

3.2. Example 2: Hexamethylbenzene Dication

The structure of hexamethylbenzene dication **2** found by ω B97XD/cc-pVTZ is a pentagonal pyramid, in which a -CMe cap subtends a five-membered ring. The carbon of the cap could be considered hexacoordinate, and termed hcC. The crystal structure has been reported [43] along with proton and C-13 NMR. Bonding is characterized by NICS [44] the system displays three-dimensional aromaticity. Apical to basal CC bond orders are small (ca. 0.5), and the apical (hexa-coordinate) Carbon employs only four electrons in bonding. That is, the octet rule is not violated.

3.2.1. AIM Analysis

Figure 7 shows bond critical points and bond paths reinforcing the concept that the cap -CCH₃ interacts with all five of the carbons in the pentagonal base. Similarly, CC bond paths define bonding between neighboring C atoms in the pentagonal base and their attachment to methyl groups. Each face of the pentagonal pyramid contains a ring critical point (RCP).

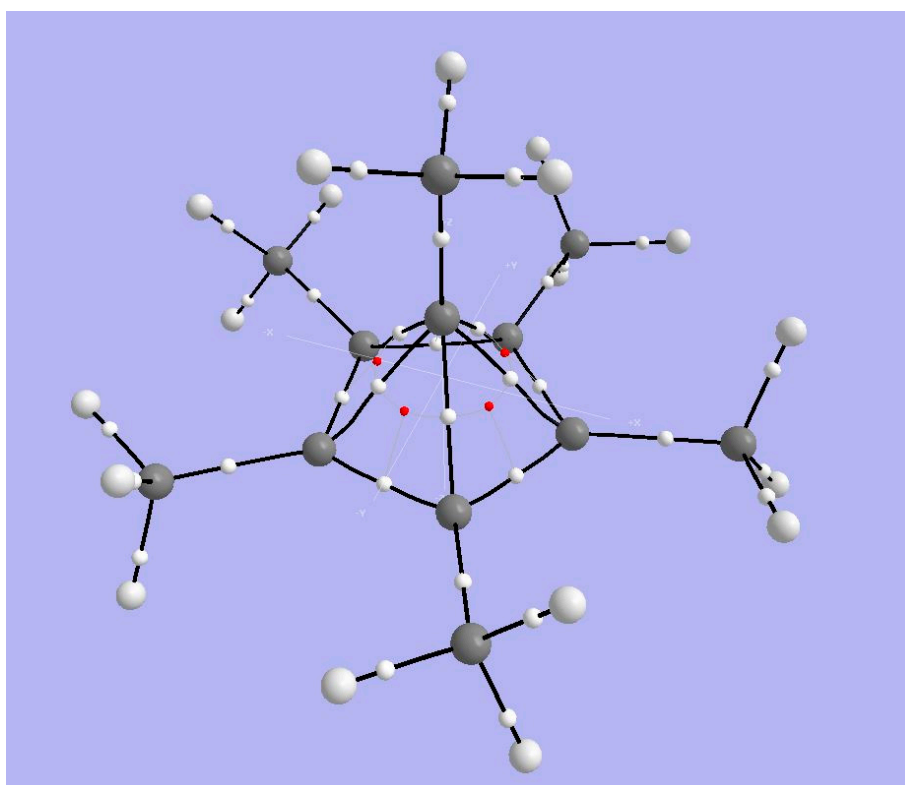


Figure 7. Topological (Bader) analysis of hexamethylbenzene **2**. Large light-gray spheres = H atoms; large dark gray spheres = C atoms; small white spheres = BCPs; small red spheres = RCPs; black lines = bond paths.

The values of the Laplacian at AIM bond critical points (shown in Table 2) suggest that the C (ring or apex) to C (methyl) bonds are conventional single bonds (the Laplacian is about -0.5 , density about 0.27) while the CC bonds within the ring are appreciably stronger, (the Laplacian is about -0.8 , density about 0.28). The BCPs for the bonds from apical C to ring Cs are distinct; density is about half that of the single covalent bonds just mentioned and the Laplacian >0 , suggesting that charge is expelled from that region, covalency is weak, and there is some electrostatic component to the interaction. Klein, Havenith, and Knizia [45] consider the compound to be best characterized as a donor-acceptor complex of anionic cyclopentadiene and a “highly Lewis-acidic Carbon atom . . . capable of acting as an electron-pair donor to a formal CH_3^+ group.” This is an appealing way to describe the bonding partly because it lends itself so well to interpretation of bonding by means of an interaction diagram. The result of charge migration, as expressed in the basin charges of AIM, is to produce the base ring of five C atoms with associated basin charges near 6.02 electrons ($|e|$) on average, with an outer ring of five methyl C atoms with basin charges near 6.037 on average. The basin charge corresponding to the apical six-coordinate C atom is 6.088 , and its methyl C basin charge is 6.016 ($|e|$). That is, even in this dication the C frame is net negative in charge. The positive charge making up the net $+2$ is borne by H atoms.

Table 2. Selected Atoms in Molecules (AIM) parameters for hexamethylbenzene dication.

Critical Point	Density	Laplacian	G	V	2G/V
C ring-C apex: (3, -1)	0.1551	+0.0205	+0.0913	-0.1765	1.0346
C ring-C ring (3, -1)	0.2823	-0.7869	+0.0894	-0.3766	0.4748
C apex-Me (3, -1)	0.2705	-0.5607	+0.0962	-0.3254	0.5913
C ring-Me (3, -1)	0.2722	-0.6231	+0.0819	-0.3194	0.5128
Basin Charges					
Charge (e)	hcC	Ring C	Apical methyl C	Ring methyl C	
	-0.088	-0.019	-0.016	-0.037	

3.2.2. ELF Analysis

Figure 8 displays the electron localization function (ELF) surface from an elevation toward a face of the pentagonal pyramid (top left) and a view from the pentagonal base (top right). The former view reveals a bond connecting the apical carbon to the carbon of its methyl, and the region of the bonding around the carbon five membered ring. The latter view shows base CC bonds, bonds from those base-plane Carbons to their methyl carbons, and the visible portions of the associated CH bonds. The apical C atom is visible in the center.

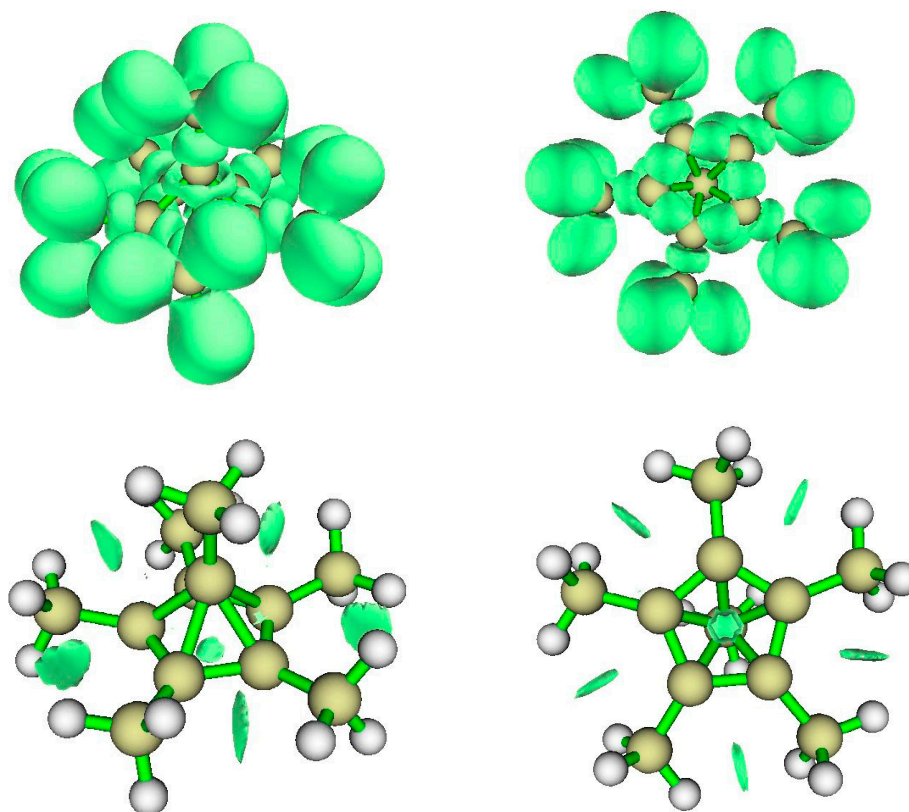


Figure 8. Views of the electron localization function isosurfaces (**top**) and the non-covalent interaction zones (**bottom**); views from an elevation toward a face of the pentagonal pyramid (**left**) and from below the base (**right**).

3.2.3. NCI Analysis

Figure 8 (bottom) displays non-covalent interaction zones for hexamethyl benzene dication. These include repulsions between adjacent methyl groups in the $(\text{CH}_3\text{C})_5$ base ring, and a feature at

the center of that ring. The plot of the reduced density gradient (RDG) $s(\rho)$ vs. the signed density (Supplementary Materials) suggests that the NCI zones identify two kinds of weak van der Waals interactions, which we can see are the ring methyl-methyl interactions and the NCI zone at the center of the five-carbon ring.

3.3. Example 3: Dimethanospiro[2.2]octaplane

To our knowledge there is no experimental realization of the C_5H_4 dication **1** itself, but Radom's ways of stabilizing this structure by steric constraint and charge delocalization might point the way toward a synthesis. The dimethanospiro[2.2]octaplane dication **3** discussed above contains a tetracoordinate planar Carbon (tpC) similar in structure to the spiropentadiene dication. The central CC_4 fragment is forced toward planarity primarily by the surrounding rigid cage structure. The constraint is most effective for the dication, and the stable minimum has D_{2h} symmetry

3.3.1. AIM Analysis

Figure 9 displays bond critical points, (white), ring critical points (red) and cage critical points (blue). The Bader parameters for cage CC and CH bond critical points (Table 3) are characteristic of saturated hydrocarbons. Note that there are bond critical points and bond paths between two pairs of C atoms coordinated to the tpC, consistent with the rectangular arrangement and the overall D_{2h} symmetry, as in spiropentadiene dication **1**. As in the case for **1**, the tpC has a negative AIM basin charge ($-0.165 |e|$); the positive charge in this dication is dispersed not substantially to the surrounding C atoms in the C_5 plane ($+0.028 |e|$ each) but rather mainly to the constraining cage atoms.

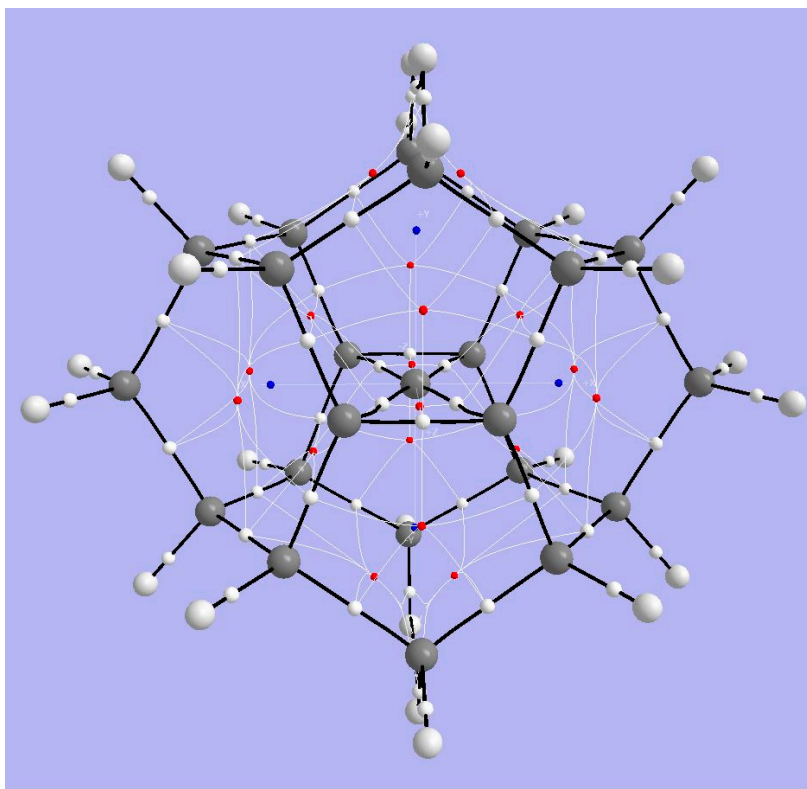


Figure 9. Topological analysis of Radom's dimethanospiro[2.2]octaplane **3**. Large light-gray spheres = H atoms; large dark gray spheres = C atoms; small white spheres = Bond CPs; small red spheres = Ring CPs; small blue spheres = Cage CPs; black lines = bond paths.

Table 3. Selected Bader parameters for Radom's dimethanospiro[2.2]octaplane dication **3**.

Critical Point	Density	Laplacian	G	V	$ -2G/V $
rC–tcC: (3, –1)	0.2286	–0.2823	+0.1435	–0.3576	0.8026
rC–rC (3, –1)	0.2981	–0.8509	+0.1084	–0.4295	0.5048
sC–sC (3, –1)	0.2493	–0.6234	+0.0729	–0.3016	0.4834

3.3.2. ELF Analysis

The ELF isosurface diagram shown in Figure 10 (left) reveals the essentially covalent character of the bonds of tpC to its neighbors and the absence of localized charge perpendicular to the plane containing the tpC and its four bonded C atoms. The lack of localized pi charge at tpC is the consequence of double ionization to the dication.

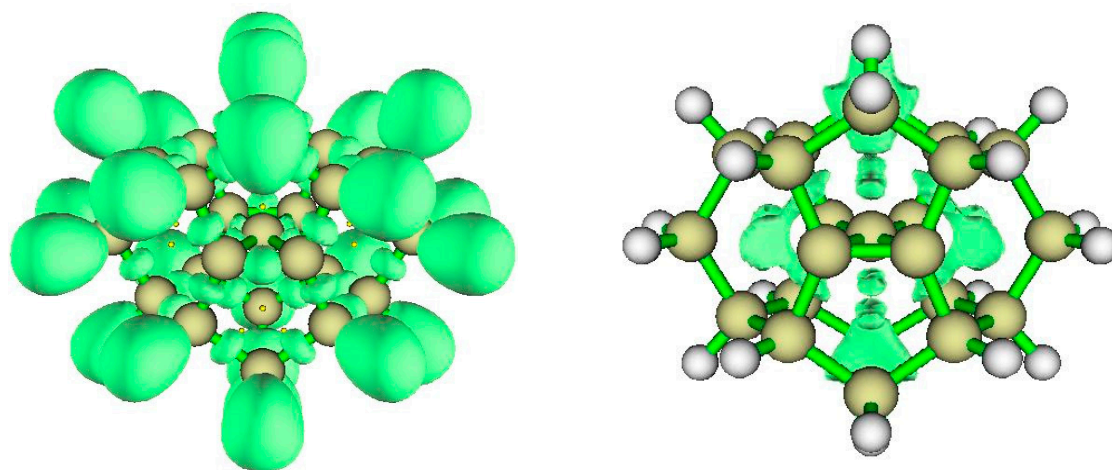


Figure 10. ELF for Radom's D_{2h} dimethanospiro[2.2]octaplane **3**, (left) showing central tpC and its bonds to its neighbors. The NCI zones (right) reveal the non-covalent interactions within the rings.

3.3.3. NCI Analysis

The plot of the reduced density gradient (RDG) $s(\rho)$ vs. the signed density (Supplementary Materials) shows van der Waals features and also strongly repulsive interaction. The NCI zones shown in Figure 10 (right) lie at cage critical points and between the $>CH_2$ bridges of the cyclooctane fragments at top and bottom of the structure. Curious NCI zones appear above and below the CC4 central plane.

3.4. Example 4: 1,8-Dimethoxy-9-Dimethoxymethylanthracene Cation

Akiba and co-workers [46–48] have reported synthesis and isolation of a compound with roughly trigonal bipyramidal five-coordinated carbon (tbpC). The C_{2v} -symmetric structure from ω B97XD/cc-pVTZ is shown in Figure 1 as species **4**. The X-ray analysis shows that the distance between the Anthryl methoxy Oxygen and the cationic 5-coordinated tbpC (2.44 ± 0.01 Å) is smaller than the distance between the ipso carbons of anthracene to which they are attached (2.50 ± 0.02 Å). Computational characterization [40] of the system also reflects a shortening, which suggests an attractive MeO...tbpC electrostatic interaction.

3.4.1. AIM Analysis

Figure 11 shows BCPs and RCPs for 1,8-dimethoxy-9-dimethoxymethylanthracene cation (species **4** in Figure 1). The broken lines representing bond paths connecting anthryl-methoxy oxygens and the

tbpC indicate a weak interaction. The Bader parameters for BCPs (Table 4) bear out the expectation that the interaction between MeO and tbpC is ionic. The Laplacian's positive sign shows that charge is exported from the BCP, and the $|2G/V|$ ratio indicates that the interaction is not covalent. We have already suspected from the short distance between methoxy O and tbpC that the tbC cationic center exerts an electrostatic attraction on the methoxy oxygens. The basin charges for the tbpC (+1.539) and methoxy oxygens (−0.140) are consistent with this inference.

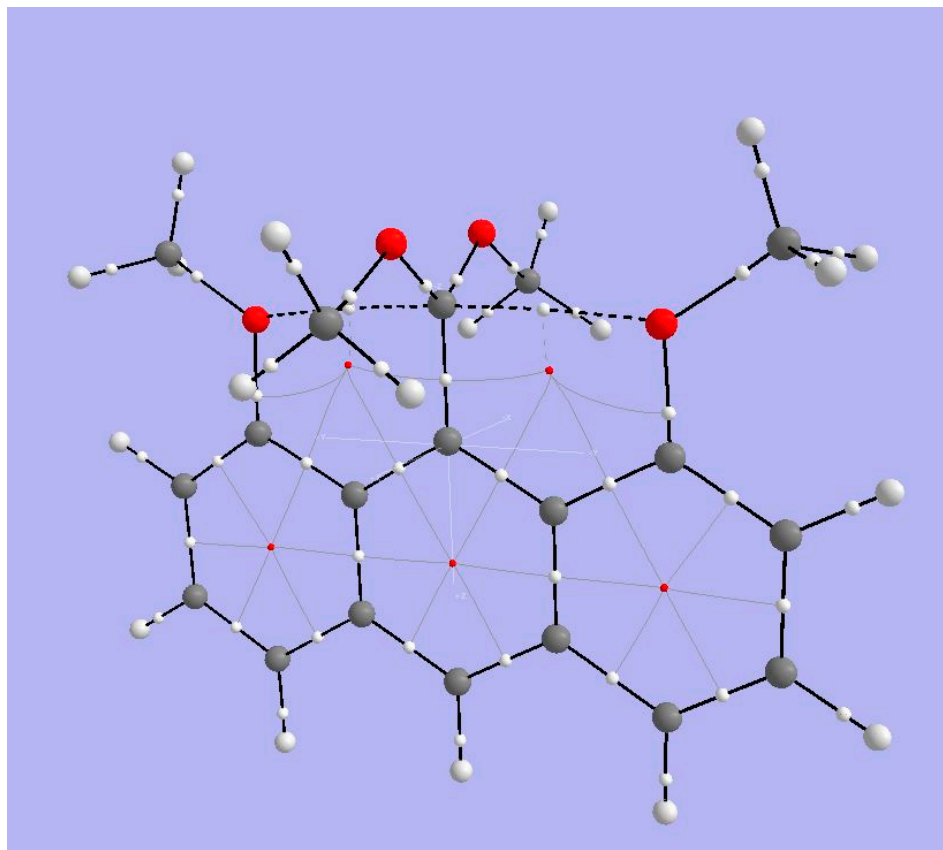


Figure 11. Topological analysis of Akiba's five-coordinate Carbon compound 4. Large light-gray spheres = H atoms; large dark gray spheres = C atoms; small white spheres = Bond CPs; small red spheres = Ring CPs; solid black lines = bond paths; broken black lines = bond paths for weak interactions.

Table 4. AIM features for 5C carbon; red entries from Akiba et al. obtained with the B3LYP/6-31G(d) model.

Critical Point	Density	Laplacian	G	V	$ 2G/V $
tbpC-OMe: (3, −1)	0.3537	−0.3326	+0.4764	−1.0359	0.9198
tbpC ... OMe (3, −1)	0.0235 0.022	+0.0898 +0.078	+0.0209	−0.0193	2.1658
C-O (3, −1)	0.2400	−0.6625	+0.2650	−0.5445	0.9734
C=C (3, −1)	0.2618	−1.0337	+0.0708	−0.3073	0.4608

3.4.2. ELF Analysis

The view of the ELF isosurfaces for Akiba's five-coordinated C species (Figure 12, left) shows the tbpC-OMe (the clearest view is at lower left) and the OMe connected to the anthryl ring; there is no ELF between that OMe's O atom and the tbpC. This argues for an interaction dominated by electrostatics.

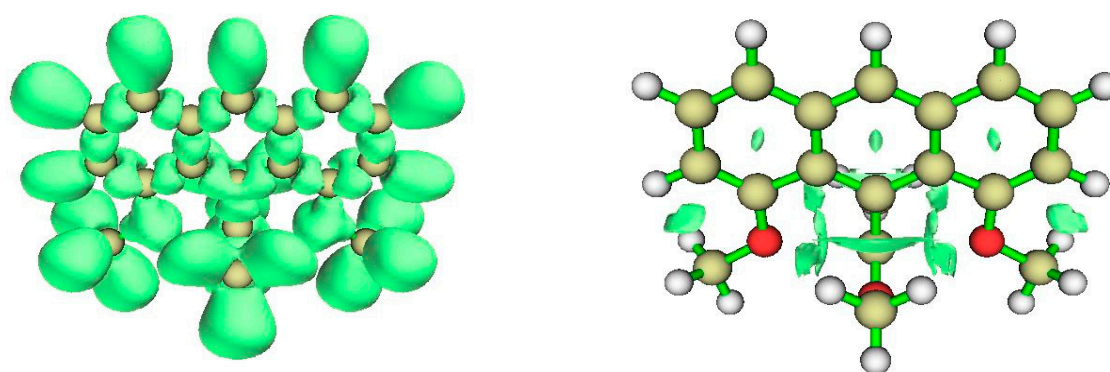


Figure 12. ELF isosurfaces and non-covalent index (NCI) zones for Akiba's five-coordinated carbon species 4.

3.4.3. NCI Analysis

The NCI regions displayed in Figure 12 (right) include the interiors of aromatic rings and the interaction zone between the anthryl methoxy fragment and a nearby CH bond. There is an NCI zone between the OMe attached to the tbpC and the anthryl Carbon to which the tbpC is attached. Most significant, we see an NCI between each anthryl methoxy O atom and the tbpC. There is important interaction, but suggests there is no covalent bonding between the anthryl methoxy O atoms and the tbpC.

4. Proposed Symmetric Variants on a Known Example of Approximately Octahedral Coordination of Carbon

Yamaguchi et al. reported the synthesis of a system with six entities in the coordination sphere of a carbon atom [49].

The design principle is shown in Figure 13. In Figure 14 showing the X-ray structure of the dication with $-SMe(+)$ bridges, (5) the golden rectangle encloses the central six-coordinate carbon (6cC) and its two allenic C neighbors, while the green arrow points to one of the four methoxy oxygen atoms in the coordination sphere of 6cC. The system is far from symmetrical, probably a consequence of packing requirements of the counterions. A variety of related hexacoordinated-C compounds have been explored computationally; for example, in the coordination sphere $-OPh$ can replace $-OMe$ as R and the bridging $>SMe(+)$ can be replaced by $>SO_2$, $>CH$, and $>S$ as B (Figure 13). Substituents can also be chosen which influence the strength of interactions in the coordination sphere [50–52].

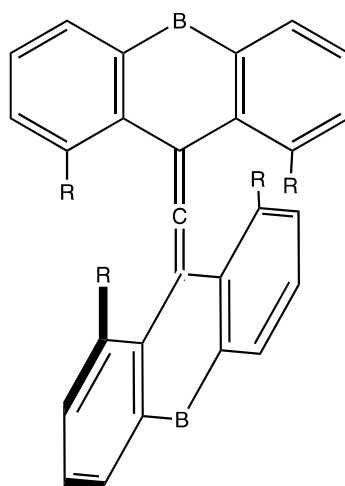


Figure 13. Design for hexacoordinate Carbon (hcC). B is a bridging group, and R is an electron donor.

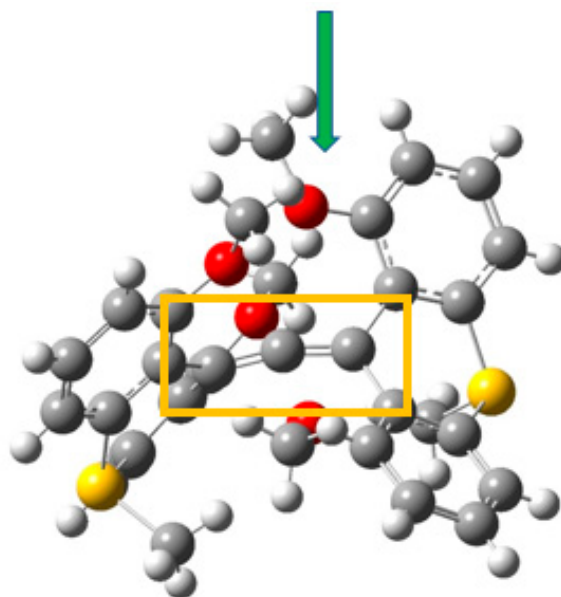


Figure 14. View of Yamaguchi's allene system with hexacoordinate carbon (species 5).

Since the behavior of this structure is complex, we address only a few details of its topology. Figure 15 displays the results of topological analysis of Yamaguchi's system, in its crystal geometry. As seen in earlier examples, bond critical points appear on bond paths (heavy black lines) corresponding to links in the molecular drawing. Ring critical points (in red) are found within each of the aromatic rings of the anthryl fragments. Fine white lines connect RCPs and BCPs. Heavy broken lines represent weaker interactions. The four methoxy oxygens are linked by such lines to the central hexacoordinate C. We also observe heavy broken lines connecting the methoxy oxygen atoms with H atoms of the thiomethyl bridging groups, among other surprising connections.

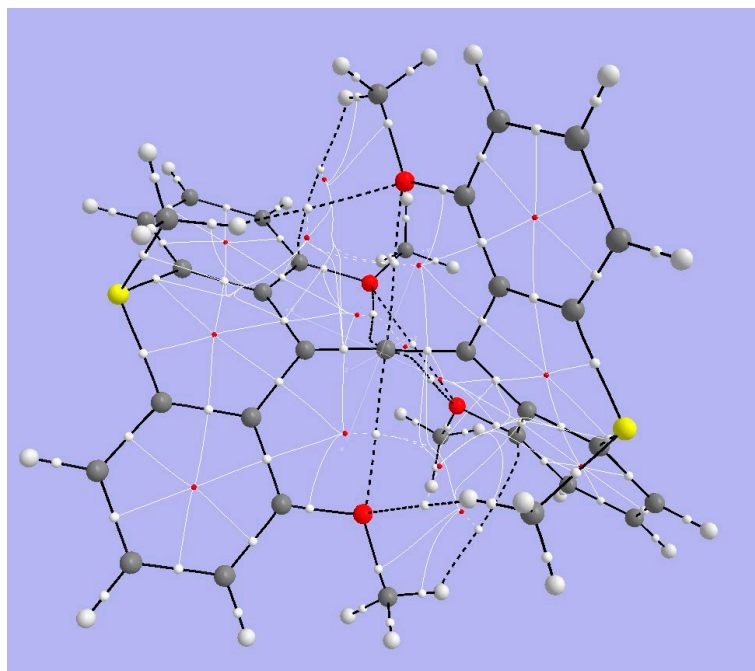


Figure 15. Bader analysis of Yamaguchi's allene. Large light-gray spheres = H atoms; large dark gray spheres = C atoms; small white spheres = Bond CPs; small red spheres = Ring CPs; solid black lines = bond paths; broken black lines = bond paths for weak interactions.

We may expect that the Bader parameters for the X-ray structure, obtained by analysis of a charge distribution that does not correspond to an energy minimum within that computational method, might be called into question. We should judge the results by their consistency with more rigorous calculations on similar systems, as described below. The density and Laplacian values at the BCPs for the allene fragment are conventional for double bonds, and the interaction between methoxy O atoms and the hcC is similar to that found in Akiba's system for its methoxy O atoms and the pcC. (Tables 4 and 5). That is, the BCPs for the bond path between MeO and the hcC have small positive $\nabla^2\rho$ values and $|2G/V|$ ratios > 1 . This indicates charge depletion at the BCP and predominantly electrostatic interactions. Since the AIM charges of these O atoms and the hcC are both negative, we can confirm that the electrostatic interaction is repulsive contrary to the suggestion that the interaction is stabilizing by mixing of the methoxy O lone pair with the allyl π^* MO and the -OMe fragments are forced into the hcC coordination sphere solely by steric constraint.

Table 5. Bader parameters for the experimental structure of Yamaguchi's hexacoordinate (hcC) system.

Critical Point	Density ρ	Laplacian $\nabla^2\rho$	Kinetic Energy Density G	Potential Energy Density V	$ 2G/V $		
Allenic hcC=Ca	+0.3444	-1.0187	+0.1551	-0.5648	0.5492		
Allenic hcC=Cb	+0.3385	-0.9761	+0.1515	-0.5470	0.5539		
CH3Oa ... hcC	+0.0182	+0.0584	+0.0128	-0.0105	2.4381		
CH3Ob ... hcC	+0.0192	+0.0739	+0.0165	-0.0146	2.2603		
CH3Oc ... hcC	+0.0140	+0.0593	+0.0155	-0.0136	2.2794		
CH3Od ... hcC	+0.0133	+0.0602	+0.0123	-0.0099	2.4848		
Basin Charges							
Atom	hcC	Allene Ca	Allene Cb	CH3Oa	CH3Ob	CH3Oc	CH3Od
AIM Q	-0.1943	+0.0926	+0.0898	-1.0736	-1.0884	-1.0753	-1.0720

Owing to the difficulty of visualization in this asymmetric system, we do not discuss the ELF and NCI figures. Instead we turn to discussion of our proposed symmetric variants.

4.1. A Neutral Symmetric System with Six-Coordinate Carbon

In the example 6 shown in Figure 16 the bridge is $>C=O$, replacing the $>SMe(+)$ of the first experimental compound 5. High symmetry allows a clearer view of the geometry of our variants. We wish to encourage synthesis of this neutral system and its $-SCH_3$ analog described below. A neutral charge allows for the possibility of high symmetry in the solid phase, thereby simplifying the X-ray analysis.

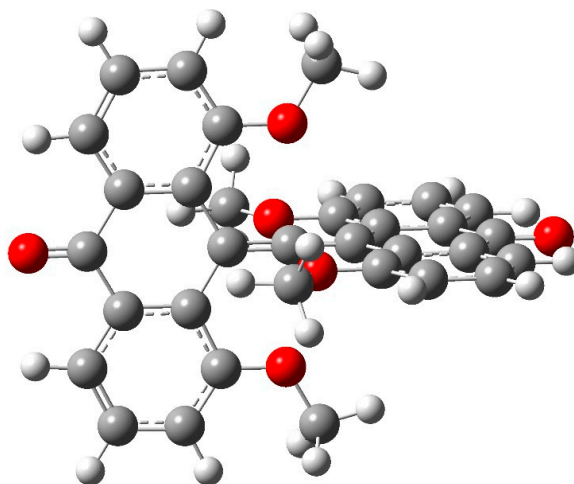


Figure 16. D_{2d} neutral symmetric variant with $>C=O$ bridge, species 6.

4.1.1. AIM Analysis

Symmetry equivalence also allows a compact presentation of AIM results, shown in Figure 17 for the $>C=O$ system 6. Some key numerical values for density, the Laplacian, and energy densities along with the ratio $|2G/V|$ are collected in Table 6. The parameters reflect the double bond character of the allenic core containing the hcC and the polar nature of the H_3C-O and $C=O$ bonds. The small values of density and the Laplacian L , and the positive sign of L as well, attest to the weak and predominantly electrostatic nature of the interaction.

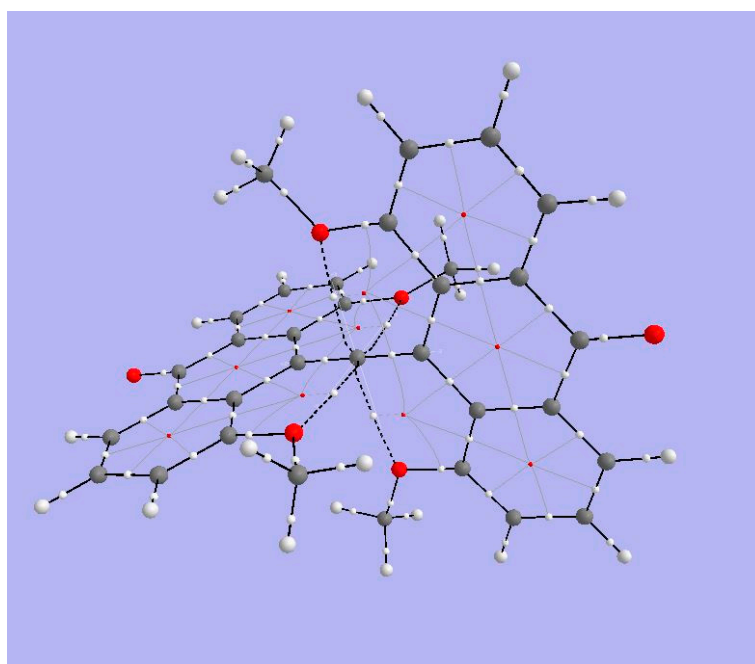


Figure 17. AIM analysis of CO system 6.

Table 6. Selected Bader parameters for D_{2d} variant (6) with $>C=O$ bridging.

Critical Point	ρ	Laplacian	G	V	$ 2G/V $
C=O bond (3, -1)	0.3976	+0.1874	+0.7174	-1.3880	1.0337
C=C bond (3, -1)	0.3455	-1.0337	+0.1576	-0.5736	0.5495
H_3C-O bond (3, -1)	0.2523	-0.2481	+0.3985	-0.6692	1.1910
MeO...C (3, -1)	0.0203	+0.0755	0.0171	-0.0154	2.2207

4.1.2. ELF Analysis

The electron localization function (Figure 18) shows the central allene system, with the anthryl methoxy oxygens in the coordination sphere of the hexacoordinated C. There is no indication of ELF amplitude in the bonding region between CH_3O and the hcC, but rather an accumulation of charge on the methoxy oxygen and depletion of charge near the hcC. This is entirely consistent with the description of the interaction between MeO and hcC as weak and electrostatic, inferred from the AIM analysis.

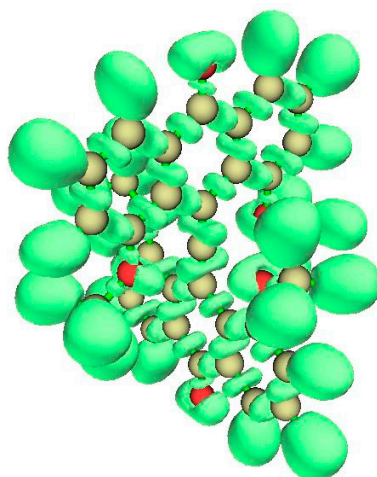


Figure 18. ELF for the D_{2d} (>CO bridge) variant of Yamaguchi's system.

4.1.3. NCI Analysis

The NCI zones displayed in Figure 19 include interactions between the bridging $>C=O$ groups and ipso CH groups of the anthryl fragments, destabilized regions within six-membered rings, and interactions between $-OCH_3$ methyl groups and nearby CH groups of the anthryl frame. Most significant for our purpose are noncovalent interactions between $-OCH_3$ and the allenyl group's central hexacoordinated carbon.

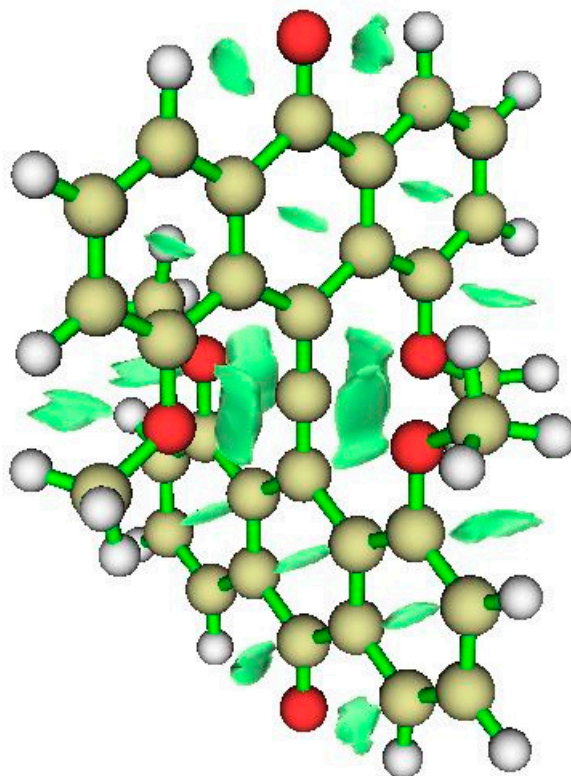


Figure 19. NCI for CO neutral variant.

4.2. A Neutral System with Attractive Interactions in the Coordination Sphere

To enhance possible soft-soft interaction between the six-coordinate Carbon and members of its coordination set we replace the methoxy O atoms by Sulfur atom, retaining D_{2d} symmetry. The structure 7 is shown in Figure 20.

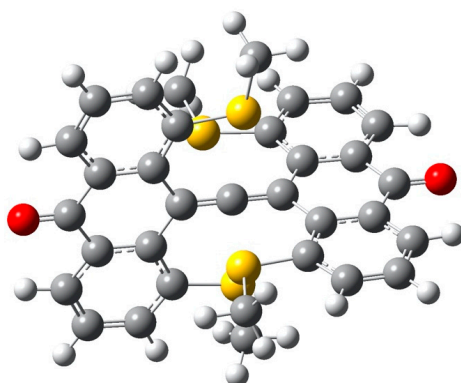


Figure 20. Structure of carbonyl-bridged system with $-\text{SCH}_3$ (7).

4.2.1. AIM Analysis

Figure 21 displays the familiar array of bond critical points (CH, CC, C=O, CS, including ring CPs for each six-membered ring). The $\text{S} \dots \text{hcC}$ bond paths are curved oddly in the neighborhood of the hcC , and there is an unexpected weak bond from anthryl CH hydrogen to $\text{S}-\text{CH}_3$ methyl carbon.

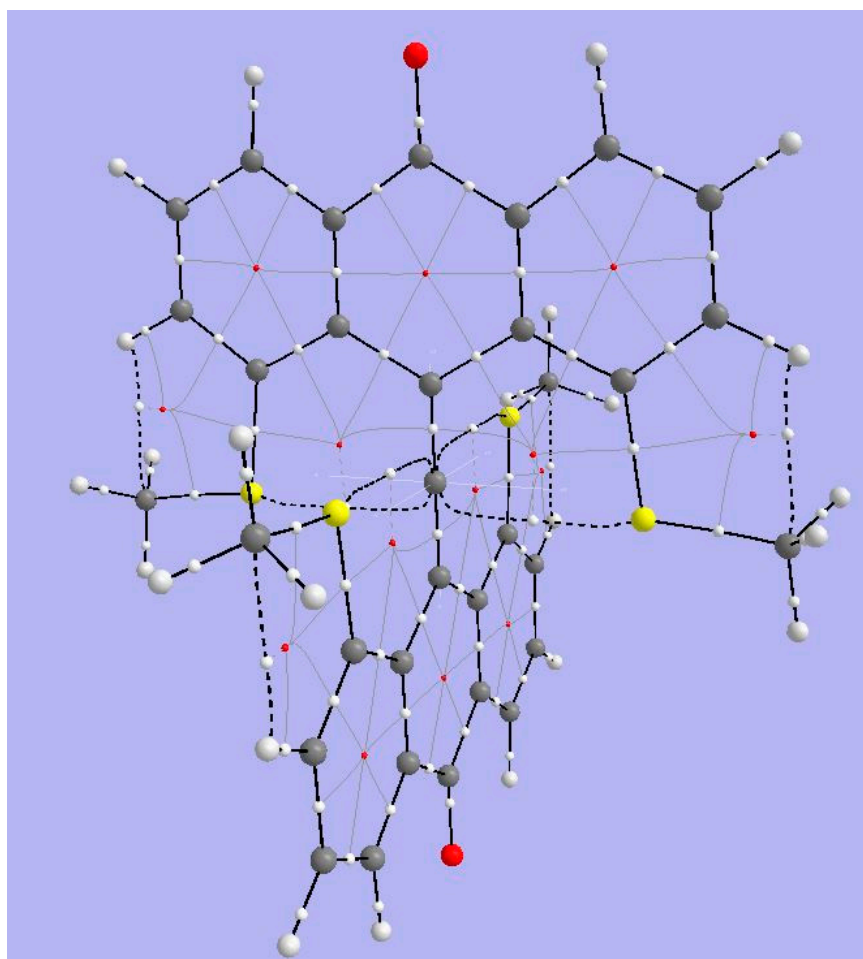


Figure 21. D_{2d} carbonyl bridge thiamethyl variant.

According to the AIM data (Table 7), the strength of the $\text{CH}_3\text{S} \dots \text{C}$ (central) interaction is almost as strong as the $\text{CH}_3\text{O} \dots \text{C}$ (central) interaction. Compare the Laplacian value of 0.0619 for 7 with +0.0755 for 6.

Table 7. Selected Bader parameters for D_{2d} thia methyl variant (7) with >C=O bridging.

Critical Point	ρ	Laplacian	G	V	2G/V
C=O bond (3, -1)	0.4045	-0.0281	+0.6700	-1.3470	0.9948
C=C bond (3, -1)	0.3448	-1.0315	+0.1624	-0.5826	0.5575
H ₃ C-S bond (3, -1)	0.1845	-0.2965	+0.0497	-0.1736	0.5726
MeS ... C (3, -1)	0.0201	+0.0619	+0.0141	-0.0128	2.3125

As was the case for the methoxy system's O ... hcC BCP, the S ... hcC BCP has a positive Laplacian, indicating charge depletion at that point, and predominantly electrostatic interaction. But in this case the interaction is attractive; hcC is negatively charged in each case, but the CH₃S sulfur atom has a positive AIM charge whereas the CH₃O oxygen atom has a strongly negative AIM charge. (Table 8) This qualitative difference is unaffected by enhancing the basis from cc-pVTZ to aug-cc-pVTZ, though the charges in the thia system are appreciably altered.

Table 8. AIM Charges for atoms in the hcC coordination zone for species 6 and 7.

Basis cc-pVTZ			
Charges (O)	C(allyl)	hcC	O atom
Species 6	+0.2193	-0.3279	-1.1729
Charges (S)	C(allyl)	hcC	S atom
Species 7	+0.1552	-0.3484	+0.1130
Basis aug-cc-pVTZ			
Charges (O)	C(allyl)	hcC	O atom
Species 6	+0.2213	-0.3256	-1.1815
Charges (S)	C(allyl)	hcC	S atom
Species 7	+0.2077	-0.4591	+0.1087

4.2.2. ELF Analysis

In Figure 22, the ELF is again shown as a set of isosurfaces enclosing regions of high charge localization. Along the axis linking the carbonyl oxygens and passing through the allenyl carbons we see features corresponding to the carbonyl oxygen lone pairs (top and bottom) and also the orthogonal pi bonds between the central hcC and its C neighbors in the allene. Two of the four S atoms (from anthryl -SMe substituents) are in view, at right and left. Lone pairs on S atoms are prominent, but there is no evident localization between S atoms and the hcC. This is consistent with the low value of electron density at the BCP on the path from S to hcC, and confirms the essentially electrostatic nature of the interaction.

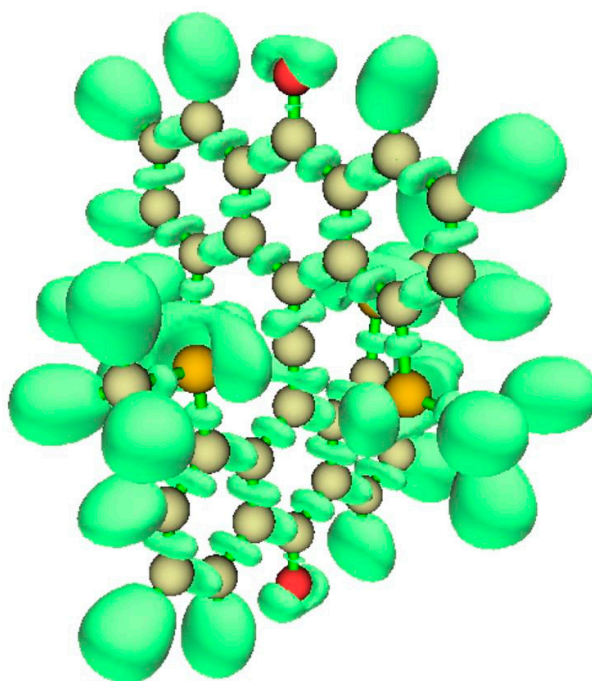


Figure 22. ELF visualization for thia variant. Oxygen atoms are shown in red, sulfur atoms in brown, and carbon atoms in gray.

4.2.3. NCI Analysis

In Figure 23, we find regions of non-covalent interaction (a) between anthryl carbonyl groups and nearby anthryl CH hydrogen atoms; (b) between $-SCH_3$ methyls and nearby anthryl CH hydrogens; and (c) within anthryl rings. Most prominent are the NCI regions between S atoms and the central hcC.

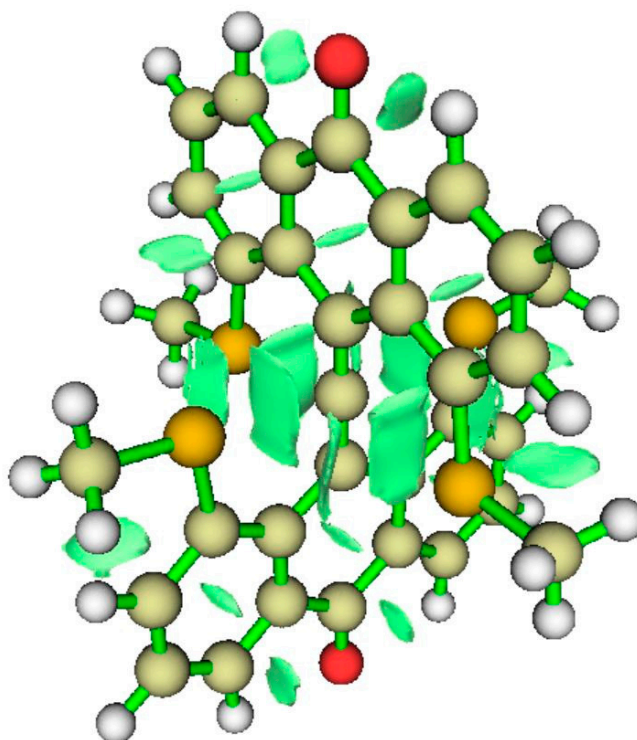


Figure 23. NCI for the thia variant.

5. Conclusions

We examined some well-established examples of unusual coordination of carbon atom. Systems **1** and **3** containing tetracoordinate planar carbon (tpC) are stabilized by removal of two electrons; in Radom's octaplanes the tpCC_4^{2+} fragment is further constrained by surrounding hydrocarbon rings. To our knowledge no X-ray structures are known for these systems, though many analogs with metal substituents have been characterized. [17–21] We recommend that the synthesis and spectroscopic characterization of hydrocarbon octaplanes be re-visited.

A signal experimental success is the structural study of hexamethyl benzene dication containing hexacoordinated carbon at the apex of a pentagonal pyramid. Bond paths confirm hexacoordination, but need not correspond to electron pair bonds. This electron-deficient species, like many carbocations with unusual carbon coordination, does not threaten the octet rule.

Building on a theme first illustrated in a cationic 1,8-dimethoxy-9-dimethoxymethylanthracene, a series of five- and six-coordinated species have been synthesized [46–50]. In the pentacoordinate system two of the O atoms in the coordination sphere are bound weakly. AIM, ELF, and NCI analysis all confirm that for an experimental system possessing six entities in a C atom's coordination sphere, and for symmetrized variations proposed here, there is evidence for six significant interactions between the allenyl central C and neighbors. The four interactions with O (**6**) or S (**7**) are electrostatic, not covalent, in view of the low level of charge sharing and density at the bond critical points. The C is hexacoordinate but not hexavalent. Again, no violation of the octet rule model is claimed.

Replacing the oxygen in the methoxy group with sulfur alters the electrostatic interaction from repulsive to attractive. We encourage synthesis of species **6** and **7**, and a thorough structural characterization including X-ray, vibrational, and NMR spectra. This should distinguish the repulsive character in **6** from the attractive character of **7**.

Supplementary Materials: The following are available online. Analysis of the $D_{2d} > \text{CF}(+)$ bridged hcC species, Plots of RDG vs λ_2 -signed density for Structures 1–4. Analysis of the $D_{2d} > \text{SO}_2$ bridged species. Cartesian coordinates for species 1–4, **6**, and **7**.

Author Contributions: Conceptualization, C.T. and Z.A.; methodology, C.T. and Z.A.; resources, C.T. and Z.A.; writing—original draft preparation, C.T.; writing—review and editing, C.T. and Z.A.; visualization, C.T. and Z.A. Software and computations, C.T., Z.A. and E.A.B. All authors have read and agreed to the published version of the manuscript.

Funding: This research received no external funding.

Acknowledgments: We thank BAPKO, the research support office of Marmara University, for financial support which allowed purchase of computing equipment. Thanks as well to the Body Foundation which made possible the acquisition of software and supported travel.

Conflicts of Interest: The authors declare no conflict of interest.

References

1. Hoff, V.J.H. Sur les formules de structure dans l'espace. *Arch. Néerl. Sci. Exact. Nat.* **1874**, *9*, 445–454.
2. Le Bel, J.A. Sur les relations qui existent entre les formules atomiques des corps organiques et le pouvoir rotatoire de leurs dissolutions. *Bull. Soc. Chim. Fr.* **1874**, *22*, 337–347.
3. Leicester, H.M. Le Bel, Joseph.Achille. In *Dictionary of Scientific Biography*; Gillispie, C.C., Ed.; Charles Scribner's Sons: New York, NY, USA, 1973; Volume 8, pp. 109–110.
4. Snelders, H.A.M. van't Hoff, Jacobus Hendricus. In *Dictionary of Scientific Biography*; Gillispie, C.C., Ed.; Charles Scribner's Sons: New York, NY, USA, 1976; Volume 13, pp. 575–581.
5. Gillespie, R.J.; Nyholm, R.S. Inorganic Stereochemistry. *Quart. Rev. Chem. Soc.* **1957**, *11*, 339–380. [[CrossRef](#)]
6. Gillespie, R.J. Fifty years of the VSEPR model. *Coord. Chem. Rev.* **2008**, *252*, 1315–1327. [[CrossRef](#)]
7. Hoffmann, R.; Alder, R.W.; Wilcox, C.F., Jr. Planar Tetracoordinate Carbon. *J. Am. Chem. Soc.* **1970**, *92*, 4992–4993. [[CrossRef](#)]
8. Hoffmann, R. The Theoretical Design of Novel Stabilized Systems. *Pure. Appl. Chem.* **1970**, *28*, 181–194. [[CrossRef](#)]

9. Wong, M.W.; Radom, L. Methane Dication: Planar but Not Square. *J. Am. Chem. Soc.* **1989**, *111*, 1155–1156. [CrossRef]
10. Lammertsma, K.; Schleyer, P.v.R. Structures and energies of isomeric carbocations ($C_5H_4^{2+}$ and $C_6H_4^{2+}$). *J. Phys. Chem.* **1988**, *92*, 881–886. [CrossRef]
11. Hogeveen, H.; Kwant, P.W. Direct observation of a remarkably stable dication of unusual structure: $(CCH_3)_6^{2+}$. *Tetrahedron Lett.* **1973**, *14*, 1665–1670. [CrossRef]
12. Hogeveen, H.; Kwant, P.W.; Postma, J.; van Duynen, P.T. Electronic spectra of pyramidal dications, $(CCH_3)_6^{2+}$ and $(CH)_6^{2+}$. *Tetrahedron Lett.* **1974**, *15*, 4351–4354. [CrossRef]
13. Hogeveen, H.; Kwant, P.W. Chemistry and spectroscopy in strongly acidic solutions XL. $(CCH_3)_6^{2+}$ an unusual dication. *J. Am. Chem. Soc.* **1974**, *96*, 2208–2214. [CrossRef]
14. Radom, L.; Rasmussen, D.R. The planar carbon story. *Pure Appl. Chem.* **1998**, *70*, 1977–1984. [CrossRef]
15. Lyons, J.E.; Rasmussen, D.R.; McGrath, M.P.; Nobes, R.H.; Radom, L. Octaplane: A Saturated Hydrocarbon with a Remarkably Low Ionization Energy Leading to a Cation with a Planar Tetracoordinate Carbon Atom. *Angew. Chem. Int. Ed. Engl.* **1994**, *33*, 1667–1668. [CrossRef]
16. Wang, Z.X.; Von Ragué Schleyer, P. The Theoretical Design of Neutral Planar Tetracoordinate Carbon Molecules with $C(C)_4$ Substructures. *J. Am. Chem. Soc.* **2002**, *124*, 11979–11982. [CrossRef] [PubMed]
17. Von Ragué Schleyer, P.; Boldyrev, A.I. A new, general strategy for achieving planar tetracoordinate geometries for carbon and other second row periodic elements. *J. Chem. Soc. Chem. Comm.* **1991**, 1536–1538. [CrossRef]
18. Li, X.; Wang, L.S.; Boldyrev, A.I.; Simons, J. Tetracoordinated planar carbon in the Al_4C -anion. A combined photoelectron spectroscopy and ab initio study. *J. Am. Chem. Soc.* **1999**, *121*, 6033–6038. [CrossRef]
19. Boldyrev, A.I.; Simons, J. Tetracoordinated Planar Carbon in Pentaatomic Molecules. *J. Am. Chem. Soc.* **1998**, *120*, 7967–7972. [CrossRef]
20. Keese, R. Carbon Flatland: Planar Tetracoordinate Carbon and Fenestranes. *Chem. Rev.* **2006**, *106*, 4787–4808. [CrossRef]
21. Wu, X.-F.; Cheng, Y.-X.; Guo, J.-C. CLi_2AlE ($E = P, As, Sb, Bi$): Planar Tetracoordinate Carbon Clusters with 16 and 14 Valence Electrons. *ACS Omega* **2019**, *4*, 21311–21318. [CrossRef]
22. Exner, K.; Schleyer, P.v.R. Planar Hexacoordinate Carbon: A Viable Possibility. *Science* **2000**, *290*, 1937–1940. [CrossRef]
23. Bader, R.F.W. *Atoms in Molecules: A Quantum Theory*, 1st ed.; Oxford University Press: Oxford, UK, 1994.
24. Becke, A.D.; Edgecombe, K.E. A simple measure of electron localization in atomic and molecular systems. *J. Chem. Phys.* **1990**, *92*, 5397–5403. [CrossRef]
25. Johnson, E.R.; Keinan, S.; Mori-Sánchez, P.; Contreras-García, J.; Cohen, A.J.; Yang, W. Revealing noncovalent interactions. *J. Am. Chem. Soc.* **2010**, *132*, 6498–6506. [CrossRef] [PubMed]
26. Frisch, M.J.; Trucks, G.W.; Schlegel, H.B.; Scuseria, G.E.; Robb, M.A.; Cheeseman, J.R.; Scalmani, G.; Barone, V.; Petersson, G.A.; Nakatsuji, H.; et al. *Gaussian 09, Revision A.02*; Gaussian, Inc.: Wallingford, CT, USA, 2016.
27. Frisch, M.J.; Trucks, G.W.; Schlegel, H.B.; Scuseria, G.E.; Robb, M.A.; Cheeseman, J.R.; Scalmani, G.; Barone, V.; Petersson, G.A.; Nakatsuji, H.; et al. *Gaussian 16, Revision C.01*; Gaussian, Inc.: Wallingford, CT, USA, 2016.
28. Chai, J.-D.; Head-Gordon, M. Long-range corrected hybrid density functionals with damped dispersion corrections. *Phys. Chem. Chem. Phys.* **2008**, *10*, 6615–6620. [CrossRef] [PubMed]
29. Dunning, T.H. Gaussian basis sets for use in correlated molecular calculations. I. The atoms boron through neon and hydrogen. *J. Chem. Phys.* **1989**, *90*, 1007–1023. [CrossRef]
30. Todd, A.; Keith, T.K. *AIMAll, Version 17.11.14*; Gristmill Software: Overland Park, KS, USA, 2017.
31. Lu, T.; Chen, F. Multiwfn: A Multifunctional Wavefunction Analyzer. *J. Comp. Chem.* **2012**, *33*, 580–592. Available online: <http://sobereva.com/multiwfn/> (accessed on 21 August 2020). [CrossRef]
32. Contreras-García, J.; Johnson, E.R.; Keinan, S.; Chaudret, R.; Piquemal, J.P.; Beretan, D.; Yang, W. NCIPlot: A program for plotting noncovalent interaction regions. *J. Chem. Theory Comp.* **2011**, *7*, 625–632.
33. Kumar, P.S.V.; Raghavendra, V.; Subramanian, V.J. Bader's theory of atoms in molecules (AIM) and its applications to chemical bonding. *J. Chem. Sci.* **2016**, *128*, 1527–1536. [CrossRef]
34. Grabowski, S.J. What is the Covalency of Hydrogen Bonding? *Chem. Rev.* **2011**, *111*, 2597–2625. [CrossRef]
35. Grimme, S.; Mueck-Lichtenfeld, C.; Erker, G.; Kehr, G.; Wang, H.; Beckers, H.; Willner, H. When do interacting atoms form a chemical bond? Spectroscopic measurements and theoretical analyses of dideuteriophenanthrene. *Angew. Chem. Int. Ed.* **2009**, *48*, 2592–2595. [CrossRef]
36. Bader, R.F.W. Bond Paths are Not Chemical Bonds. *J. Phys. Chem. A* **2009**, *113*, 10391–10396. [CrossRef]

37. Cerpa, E.; Andreas Krapp, A.; Flores-Moreno, R. Influence of Endohedral Confinement on the Electronic Interaction between He atoms: A He₂@C₂₀H₂₀ Case Study. *Chem. Eur. J.* **2009**, *15*, 1985–1990. [[CrossRef](#)]
38. Clark, T.; Murray, J.S.; Politzer, P. A perspective on quantum mechanics and chemical concepts in describing noncovalent interactions. *Phys. Chem. Chem. Phys.* **2018**, *20*, 30076–30082. [[CrossRef](#)]
39. Narth, C.; Maroun, Z.; Boto, C.R.; Bonnet, M.-L.; Piquemal, J.-P.; Contreras-Garcia, J. A Complete NCI Perspective from new bonds to reactivity. In *Applications of Topological Methods in Molecular Chemistry*; Alikhani, E., Chauvin, R., Lepetit, C., Silvi, B., Eds.; Springer: Berlin, Germany, 2016; Volume 22, pp. 491–527.
40. Esteves, P.M.; Ferreira, N.B.P.; Corrêa, R.J. Neutral Structures with a Planar Tetracoordinated Carbon Based on Spiropentadiene Analogues. *J. Am. Chem. Soc.* **2005**, *127*, 8680–8685. [[CrossRef](#)] [[PubMed](#)]
41. Firme, C.L.; Barreiro, N.B.P.; Esteves, P.M.; Corrêa, R.J. Understanding the Planar Tetracoordinate Carbon Atom: Spiropentadiene Dication. *J. Phys. Chem. A* **2008**, *112*, 686–692. [[CrossRef](#)] [[PubMed](#)]
42. Firme, C.L.; Antunes, O.A.C.; Esteves, P.M.; Corrêa, R.J. Derivatives of Spiropentadiene Dication: New Species with Planar Tetracoordinate Carbon (ptC) atom. *J. Phys. Chem. A* **2009**, *113*, 3171–3176. [[CrossRef](#)] [[PubMed](#)]
43. Malischewski, M.; Seppelt, K. Crystal Structure Determination of the Pentagonal-Pyramidal Hexamethylbenzene Dication (CH₃)₆C₆²⁺. *Angew. Chem. Int. Ed.* **2017**, *56*, 368–370. [[CrossRef](#)] [[PubMed](#)]
44. Schleyer, P.v.R.; Maerker, C.; Dransfeld, A.; Jiao, H.; van Eikema Hommes, N.J. Nucleus-Independent Chemical Shifts: A Simple and Efficient Aromaticity Probe. *J. Am. Chem. Soc.* **1996**, *118*, 6317–6318. [[CrossRef](#)]
45. Klein, J.E.M.N.; Havenith, R.W.A.; Knizia, G. The Pentagonal-Pyramidal Hexamethylbenzene Dication: Many Shades of Coordination Chemistry at Carbon. *Chem. Eur. J.* **2018**, *24*, 12340–12345. [[CrossRef](#)]
46. Akiba, K.; Yamashita, M.; Yamamoto, Y.; Nagase, S. Synthesis and Isolation of Stable Hypervalent Carbon Compound (10-C-5) Bearing a 1,8-Dimethoxyanthracene Ligand. *J. Am. Chem. Soc.* **1999**, *121*, 10644–10645. [[CrossRef](#)]
47. Yamamoto, Y.; Akiba, K. Synthesis of Hypervalent Pentavalent Carbon and Boron Compounds. *J. Synth. Org. Chem. Jpn.* **2004**, *62*, 1128–1137. [[CrossRef](#)]
48. Yamashita, M.; Yamamoto, Y.; Akiba, K.; Hashizume, D.; Iwasaki, F.; Tagaki, N.; Nagase, S. Synthesis and Structures of Hypervalent Carbon and Boron Compounds Bearing an Anthracene Skeleton—Elucidation of Hypervalent Interaction Based on X-ray Analysis and DFT Calculation. *J. Am. Chem. Soc.* **2005**, *127*, 4354–4371. [[CrossRef](#)] [[PubMed](#)]
49. Yamaguchi, T.; Yamamoto, Y.; Kinoshita, D.; Akiba, K.; Zhang, Y.; Reed, C.A.; Hashizume, D.; Iwasaki, F. Synthesis and Structure of a Hexacoordinate Carbon Compound. *J. Amer. Chem. Soc.* **2008**, *130*, 6894–6895. [[CrossRef](#)] [[PubMed](#)]
50. Yamaguchi, T.; Yamamoto, Y. Substituent effects on the structure of hexacoordinate carbon bearing two thioxanthene ligands. *Pure Appl. Chem.* **2013**, *85*, 671–682. [[CrossRef](#)]
51. Nakai, H.; Okoshi, M.; Atsumi, T.; Kikuchi, T.; Akiba, K. Theoretical Design of Hexacoordinate Hypervalent Carbon Compounds by Analyzing Substituent Effects. *Bull. Chem. Soc. Jpn.* **2011**, *84*, 505–510. [[CrossRef](#)]
52. Kikuchi, Y.; Ishii, M.; Akiba, K.; Nakai, H. Discovery of hexacoordinate hypervalent carbon compounds: Density functional study. *Chem. Phys. Lett.* **2008**, *460*, 37–41. [[CrossRef](#)]

